



Cite this: *Phys. Chem. Chem. Phys.*, 2022, 24, 4226

## Molecular-level electrocatalytic CO<sub>2</sub> reduction reaction mediated by single platinum atoms†

Gaoxiang Liu,<sup>‡</sup> a Isuru R. Ariyaratna,<sup>§</sup> b Zhaoguo Zhu,<sup>a</sup> Sandra M. Ciborowski,<sup>‡</sup> a Evangelos Miliordos,<sup>§</sup> \* b and Kit H. Bowen<sup>\* a</sup>

The activation and transformation of H<sub>2</sub>O and CO<sub>2</sub> mediated by electrons and single Pt atoms is demonstrated at the molecular level. The reaction mechanism is revealed by the synergy of mass spectrometry, photoelectron spectroscopy, and quantum chemical calculations. Specifically, a Pt atom captures an electron and activates H<sub>2</sub>O to form a H–Pt–OH<sup>−</sup> complex. This complex reacts with CO<sub>2</sub> via two different pathways to form formate, where CO<sub>2</sub> is hydrogenated, or to form bicarbonate, where CO<sub>2</sub> is carbonated. The overall formula of this reaction is identical to a typical electrochemical CO<sub>2</sub> reduction reaction on a Pt electrode. Since the reactants are electrons and isolated, single atoms and molecules, we term this reaction a molecular-level electrochemical CO<sub>2</sub> reduction reaction. Mechanistic analysis reveals that the negative charge distribution on the Pt–H and the –OH moieties in H–Pt–OH<sup>−</sup> is critical for the hydrogenation and carbonation of CO<sub>2</sub>. The realization of the molecular-level CO<sub>2</sub> reduction reaction provides insights into the design of novel catalysts for the electrochemical conversion of CO<sub>2</sub>.

Received 12th November 2021,  
 Accepted 31st January 2022

DOI: 10.1039/d1cp05189j

rsc.li/pccp

### Introduction

The electrocatalytic conversion of CO<sub>2</sub> into reduced, value-added molecules has received extensive attention for both environmental and economic reasons. While noble metal nanomaterials, such as Pt, Pd, Ru, Rh, and Ir, are mostly commonly used in electrocatalysis due to their high activity, their high cost and low natural abundance introduce major difficulties in using them for large-scale, industrial applications. Single-atom electrocatalysts that comprise isolated active metal centers represent a promising strategy for mitigating this issue, owing to their maximum atom efficiency and unique atomic structures and electronic properties.<sup>1–3</sup> For instance, downsizing the Pt nanoparticles to single-atoms supported on substrates improves their activities toward several electrochemical reduction processes, including hydrogen evolution reaction, oxygen reduction reaction, and CO<sub>2</sub> reduction.<sup>4,5</sup> In this

study, we explore the possibility of further reducing the scale of an electrochemical reduction reaction to the molecular level. The aim is to use electrons, isolated, single noble metal atoms, water, and CO<sub>2</sub> molecules to achieve an electrochemical CO<sub>2</sub> reduction reaction (CO<sub>2</sub>RR) that involves as few chemical entities as possible.

We selected the platinum atom as the noble metal to mediate this molecular-level electrochemical CO<sub>2</sub>RR, a choice inspired by a lineage of our recent studies. In studies related to CO<sub>2</sub> activation and functionalization, we showed that the negative ions of metal atoms, including Pt<sup>−</sup>, activate CO<sub>2</sub>,<sup>6,7</sup> and that the activated groups on Pt atom, such as the hydro and the methyl groups, functionalize CO<sub>2</sub> into formate and acetate.<sup>8,9</sup> In another study, we showed that while a neutral platinum atom is inert toward water, after adding an electron, a platinum anion activates a water molecule by breaking the O–H bond to form a H–Pt–OH<sup>−</sup> complex.<sup>10</sup> The hydro and the hydroxy groups in this complex are expected to be active in reacting with other small molecules. Based on these studies, we conceive that electrons endow Pt atoms with activities for both water activation and the CO<sub>2</sub> functionalization, and that by coupling such activities, Pt atoms can mediate a molecular-level electrochemical CO<sub>2</sub> reduction reaction. Here, we demonstrate that in the presence of electrons, Pt atoms break water molecules into –H and –OH groups, and respectively couple these two groups with CO<sub>2</sub> to form formate and bicarbonate. The overall chemical formula for this molecular-level reaction resembles that of a typical electrochemical CO<sub>2</sub>RR on a Pt

<sup>a</sup> Department of Chemistry, Johns Hopkins University, 3400 N Charles St, Baltimore, MD 21218, USA. E-mail: kbowen@jhu.edu

<sup>b</sup> Department of Chemistry and Biochemistry, Auburn University, Auburn, AL 36849, USA. E-mail: ezm0048@auburn.edu

† Electronic supplementary information (ESI) available: Fig. S1–S4; coordinates and vibrational frequencies of all structures. See DOI: 10.1039/d1cp05189j

‡ Present address: Advanced Bioimaging Center, Department of Molecular and Cell Biology, University of California, Berkeley, Barker Hall, Berkeley, CA 94720, USA.

§ Present address: Department of Chemical Engineering, Massachusetts Institute of Technology, Cambridge, MA 02139, USA.

electrode. This work demonstrates the smallest scale electrochemical  $\text{CO}_2$  reduction reaction mediated by single atoms known.

## Results and discussion

The molecular-level  $\text{CO}_2$  reduction reaction starts with the controlled activation of one O–H bond in  $\text{H}_2\text{O}$  by single Pt atoms and electrons.<sup>11</sup> Water activation occurred in a laser vaporization source, where a laser-generated plasma containing Pt atoms and electrons interacted with water molecules introduced into the vaporization chamber. The activation product,  $\text{PtH}_2\text{O}^-$ , was characterized by negative ion photoelectron spectroscopy and confirmed as  $\text{H-Pt-OH}^-$  (Fig. 1A top panel and Fig. S1, ESI<sup>†</sup>). This activation product then reacted with  $\text{CO}_2$  added into a reaction cell downstream by a second pulse valve. As all reactants were carried by supersonically expanding helium jets, the reaction temperature is estimated to be on the order of several Kelvins. The duration of the reaction is around 40  $\mu\text{s}$ , which is determined by the difference between the trigger timings of the second pulse valve and the

time-of-flight mass spectrometer. The resultant mass spectra show prominent new peaks of reaction products at the lower mass region, while a mass series of  $[\text{H-Pt-OH}(\text{CO}_2)]^-$  is observed at the higher mass region (Fig. 1A bottom panel). Here, we focus on the species with an amu lower than 280, as these species represent the possible intermediates and products resulting from the reactions among  $\text{H}_2\text{O}$ ,  $\text{CO}_2$ , and single Pt anions. Pt clusters are not expected to contribute to these reactions. The intermediates related to reactions with Pt clusters should have the molecular formula  $\text{Pt}_n(\text{H}_2\text{O})(\text{CO}_2)^-$  ( $n \geq 2$ ) with a minimum molecular weight of 450 amu, which are beyond the scope of this work.

The peaks at the lower mass region are identified as  $\text{HCO}_2^-$  (formate),  $\text{HCO}_3^-$ ,  $\text{CO}_3^-$ , and the solvation complexes of these species according to their masses and photoelectron spectra (Fig. 1B top panel and Fig. S2, ESI<sup>†</sup>). For comparison, the reaction between  $\text{H}_2\text{O}$  and  $\text{CO}_2$  with the presence of electrons only forms the  $(\text{CO}_2)_n(\text{H}_2\text{O})_m^-$  solvation complexes<sup>11</sup> (Fig. S3, ESI<sup>†</sup>). This confirms that electrons alone will not induce chemical bond breakage or reformation in a  $\text{H}_2\text{O}$  and  $\text{CO}_2$  gas expansion under our experimental conditions. Therefore, Pt atoms are critical for the formation of  $\text{HCO}_2^-$ ,  $\text{HCO}_3^-$ , and  $\text{CO}_3^-$ .  $\text{HCO}_2^-$  and  $\text{HCO}_3^-$  are likely due to the reactions between  $\text{CO}_2$  respectively with the  $-\text{H}$  and  $-\text{OH}$  groups in the water activation complex  $\text{H-Pt-OH}^-$ . The  $\text{CO}_3^-$  can be the result of electron-induced deprotonation of  $\text{HCO}_3^-$ , which is common for gas-phase acidic anions. The high intensities of these lower mass products suggest an efficient interaction between  $\text{CO}_2$  and  $\text{H-Pt-OH}^-$ .

We then characterized the  $[\text{H-Pt-OH}(\text{CO}_2)]^-$  reaction intermediate with negative ion photoelectron spectroscopy (Fig. 2). The photoelectron spectra were taken at all the mass isotopes, and no significant spectroscopic difference was observed

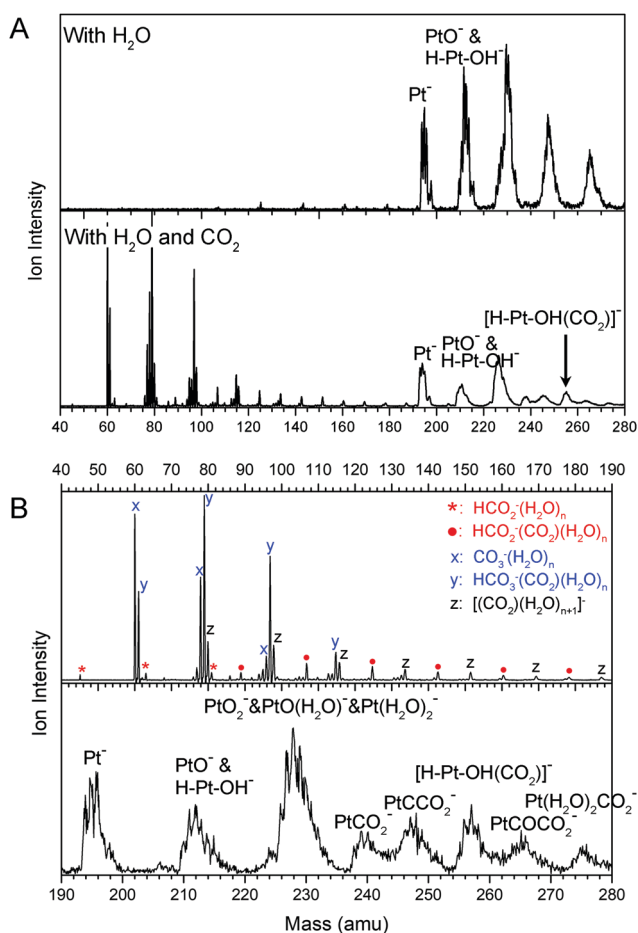


**Fig. 1** (A) Mass spectra of  $\text{Pt}^-$  reacting with  $\text{H}_2\text{O}$  (top panel) and with  $\text{H}_2\text{O}$  and  $\text{CO}_2$  (bottom panel). (B) The mass spectrum of  $\text{Pt}^-$  with  $\text{H}_2\text{O}$  and  $\text{CO}_2$  is bisected into the lower (top panel) and higher (bottom panel) mass regions for a closer view of the reaction products.

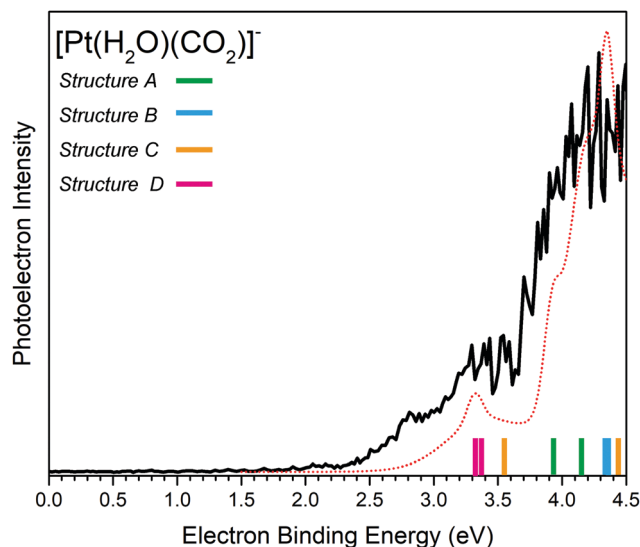


**Fig. 2** Photoelectron spectra of  $[\text{H-Pt-OH}(\text{CO}_2)]^-$  measured with 266 nm (4.661 eV) photons. The stick spectrum overlay represents the calculated VDEs of the different  $[\text{H-Pt-OH}(\text{CO}_2)]^-$  structures in Fig. 3. The dotted line represents the simulated spectrum.

among them. The  $[\text{H-Pt-OH}(\text{CO}_2)]^-$  spectrum is convolved, suggesting contributions from multiple isomers of  $[\text{H-Pt-OH}(\text{CO}_2)]^-$  that coexist in the ion beam. The photoelectron spectrum consists of two subregions. The first region is relatively weak in intensity and has multiple peaks with electron binding energy (EBE) lower than 3.6 eV. This indicates that the isomers with their vertical detachment energies (VDE), which are defined as the photodetachment transition energy at which the Franck–Condon overlap is at its maximum between the anion's vibrational wave function and that of its neutral counterpart, below 3.6 eV make up a lesser portion in the  $[\text{H-Pt-OH}(\text{CO}_2)]^-$  beam. The spectral region above 3.6 eV, on the other hand, is higher in intensity, suggesting the  $[\text{H-Pt-OH}(\text{CO}_2)]^-$  isomers with a VDE higher than 3.6 eV are the major species in the ion beam. In other words, these isomers are more stable than those with a lower VDE.

The complexity of the  $[\text{H-Pt-OH}(\text{CO}_2)]^-$  photoelectron spectrum necessitates quantum chemical calculations to identify the molecular species of this reaction intermediate. A distinct advantage for studying gas-phase reactions between single atoms and molecules is the synergy between experimental characterization and high-level quantum chemistry calculations for identifying reaction intermediates and products, which lays the foundation for mechanistic insight into the reactions at a molecular level.<sup>12</sup> We started by performing density functional theory to search for  $[\text{H-Pt-OH}(\text{CO}_2)]^-$  isomers that are possibly formed *via* the reaction between  $\text{H-Pt-OH}^-$  and  $\text{CO}_2$ . The energetics of these isomers were then refined at the CCSD(T) level of theory. The optimized geometries for these reaction intermediates are presented in Fig. 3 along with their relative energies. All energies are zero-point energy corrected. The structures of  $\text{H-Pt-OH}^-$  and  $\text{CO}_2$  are also presented for reference. All  $[\text{H-Pt-OH}(\text{CO}_2)]^-$  isomers are in a doublet electronic state. In the global minimum of  $[\text{H-Pt-OH}(\text{CO}_2)]^-$ , **A**,  $\text{CO}_2$  is wedged into the Pt–H bond of

$\text{H-Pt-OH}^-$  to form a  $\text{HOCO-Pt-OH}^-$  structure, that is,  $\text{CO}_2$  is hydrogenated to formate. In structure **B**, which is essentially isoenergetic to the global minimum,  $\text{CO}_2$  is inserted into the O–H bond of  $\text{H-Pt-OH}^-$ , forming a  $\text{H-Pt-HCO}_3^-$  structure where  $\text{CO}_2$  is carbonated. The bicarbonate is attached to the Pt atom *via* a Pt–O bond. Structures **C** and **D** are formed by the absorption of  $\text{CO}_2$  respectively onto the Pt and O atoms in  $\text{H-Pt-OH}^-$ . In structure **C**,  $\text{CO}_2$  exhibits a bent geometry. This suggests that  $\text{CO}_2$  is activated, which is the first step for  $\text{CO}_2$  to be further functionalized, upon bonding with the Pt atom. In structure **D**, on the other hand, while  $\text{CO}_2$  also appears bent, its local charge is only slightly positive after interacting with the O atom. This suggests that charge transfer in structure **D** is minimal, and  $\text{CO}_2$  is not activated. Based on the atomic connectivity, structure **C** is the prior step for forming structure **A**, while structure **D** is the essential step to generate structure **B**.

To verify these computationally optimized structures, we calculated their VDEs at the CCSD(T) level of theory and compared them with the experimental spectrum. The EBE transition below 3.6 eV results from the photodetachment transitions of structures **C** and **D**, whose calculated VDEs to their singlet neutrals are 3.54 and 3.37 eV, respectively. For structure **D**, its VDE to the triplet neutral, which is 3.32 eV, also falls into this EBE band. The EBE feature higher than 3.6 eV is due to the photodetachment transition of structures **A** and **B** to their corresponding singlet and triplet neutrals. The transition from structure **C** to its singlet also contributes to this EBE feature. We simulated the photoelectron spectrum based on the calculated electron affinities and VDEs (see Methods). The match between the simulated and experimental spectra indicates that structures **A**, **B**, **C**, and **D** all exist as the intermediates of the reaction between  $\text{H-Pt-OH}^-$  and  $\text{CO}_2$ .

The identification of the formate and bicarbonate adducts, structures **A** and **B**, and their corresponding precursors, structures **C** and **D**, suggests two possible reaction mechanisms that are respectively responsible for the formation of the formate and the bicarbonate products observed in the mass spectra. To gain a detailed mechanistic insight into how  $\text{H}_2\text{O}$  and  $\text{CO}_2$  are transformed on the anionic Pt atom, we investigated the reaction pathway with quantum chemical calculations (Fig. 4). The reaction starts with the breakage of one O–H bond  $\text{H}_2\text{O}$  by  $\text{Pt}^-$ , which has been elaborated in our previous work. This step includes a barrier of 0.51 eV and is exothermic by 1.26 eV.<sup>10</sup> The resultant  $\text{H-Pt-OH}^-$  can react with  $\text{CO}_2$  *via* a Pt/C interaction that leads to  $\text{CO}_2$  hydrogenation, or an O/C interaction that results in  $\text{CO}_2$  carbonation. The Pt/C interaction causes a 0.5 |e| negative charge transfer to  $\text{CO}_2$  and the formation of a Pt–C bond (Structure **C**). The activated  $\text{CO}_2$  then interacts with the Pt–H bond of  $\text{H-Pt-OH}^-$ . The H atom transfers to the C atom while the Pt atom binds the O atom, leading to the formation of  $\text{HO-Pt-OCOH}^-$  that contains a formate moiety (Structure **A**). The transition state, **TS1**, is located 0.05 eV below  $\text{H-Pt-OH}^-$  and  $\text{CO}_2$ , the reactants for the  $\text{CO}_2$  hydrogenation step, and 1.31 eV lower than  $\text{Pt}^-$ ,  $\text{H}_2\text{O}$ , and  $\text{CO}_2$ , which is the entrance channel of the entire reaction. Therefore,  $\text{H-Pt-OH}^-$  readily hydrogenates  $\text{CO}_2$  into the formate adduct intermediate *via* the Pt/C interaction route. Structure **A** can further dissociate into  $\text{PtOH}$  and  $\text{HCO}_2^-$ ,

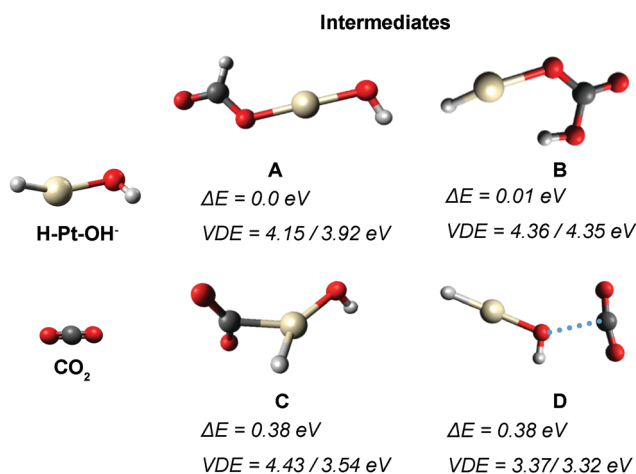


Fig. 3 Optimized structures for  $\text{H-Pt-OH}^-$ ,  $\text{CO}_2$ , and  $[\text{H-Pt-OH}(\text{CO}_2)]^-$ . The relative energies of  $[\text{H-Pt-OH}(\text{CO}_2)]^-$  and their calculated VDEs to singlet and triplet neutrals are shown below each structure. The Natural Bond Orbital (NBO) charge on each atom is also provided.

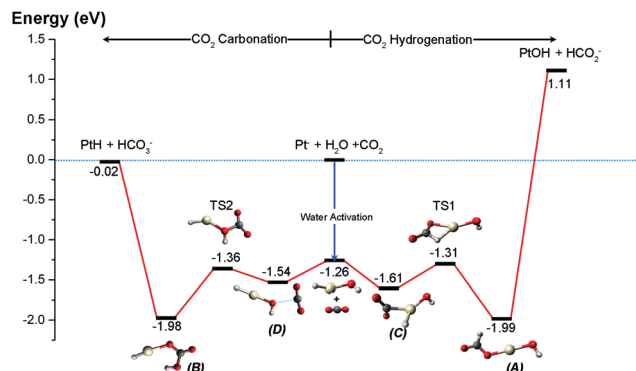
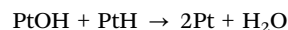
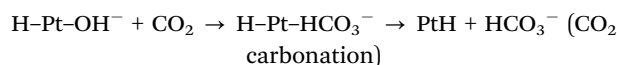
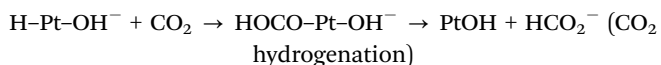
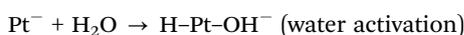
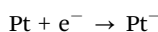


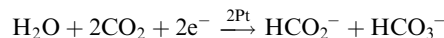
Fig. 4 Profile of the molecular-level  $\text{CO}_2\text{RR}$  mediated by anionic Pt atoms. Zero-point corrected energies are given in eV. The letters in parentheses correspond to their labels in Fig. 3. The potential energy surface is referenced to the total energy of isolated  $\text{Pt}^-$ ,  $\text{H}_2\text{O}$ , and  $\text{CO}_2$ .

accounting for the formate and formate-containing products observed in the mass spectrum. This step is endothermic, with the dissociation products 1.11 eV higher than the entrance channel. Such extra energy can be provided *via* multicollisions with the fastest He molecules in the Maxwell-Boltzmann distribution under our experimental conditions.<sup>13</sup> It is also worth noting that  $\text{H-Pt-OH}^-$  may undergo a direct reaction mechanism where its  $-\text{H}$  group transfers to  $\text{CO}_2$  to form a formate without going through the  $\text{HO-Pt-OCO}^-$  intermediate (Structure A).<sup>13a,14</sup> For the O/C interaction route, the  $\text{CO}_2$  wedges into the O-H bond of  $\text{H-Pt-OH}^-$  to form a bicarbonate adduct (Structure B) *via* TS2, which lies 1.36 eV below the entrance channel. This adduct can dissociate into PtH and  $\text{HCO}_3^-$ , whose total energy is almost identical to the entrance channel. Note that the  $\text{CO}_2$  activation intermediate, D, the transition state, TS2, and the adduct intermediate, B, in the  $\text{CO}_2$  carbonation route, are respectively similar in energy as compared to their corresponding structures, C, TS1, and A, in the  $\text{CO}_2$  hydrogenation route. Therefore, the carbonation and hydrogenation routes have alike energetic profiles before the dissociation of the reaction intermediates, and the higher energy of hydrogenation products accounts for the lower intensities of  $\text{HCO}_2^-$  related species as compared to the  $\text{HCO}_3^-$  related ones (Fig. 1).

The observation of a significant amount of formate, bicarbonate, and their related products in the mass spectrum suggests a high yield of PtH and PtOH as the reaction products, though they were not directly observed due to a lack of charge. In addition, the solvation and deprotonation of formate and bicarbonate indicate noticeable interactions among the reaction products. Therefore, PtH and PtOH may react with each other to form two Pt atoms and one  $\text{H}_2\text{O}$  molecule under our experimental conditions, completing the catalytic cycle by regenerating Pt atoms. We can thus summarize all the reaction steps as follows:



By combining and balancing these steps, we proposed that the overall reaction that occurred in our experimental setup is:



Therefore, while the reactants in our setup are electrons and isolated, single atoms and molecules, the overall reaction has the same formula as a typical electrochemical  $\text{CO}_2$  reduction reaction on a Pt electrode. We thus propose that the  $\text{H}_2\text{O}$  and  $\text{CO}_2$  activation and conversion mediated by Pt atoms and electrons in this work represents an electrochemical  $\text{CO}_2$  reduction reaction at the molecular level.

The neutral Pt atom is inactive to  $\text{H}_2\text{O}$ . With the addition of an excess electron,  $\text{Pt}^-$  activates water by breaking one of its O-H bonds to form  $\text{H-Pt-OH}^-$ . The negative charge on Pt reduces to  $-0.09 |e|$  after redistributing to the  $-\text{H}$  and the  $-\text{OH}$  groups, with the O atoms carrying the major portion of the negative charge in this water activation complex. While the negative charge on Pt in this complex is significantly lower than those observed in our previous studies, the H atom that is directly connected to Pt also contributes its negative charge when Pt interacts with  $\text{CO}_2$ . This is manifested by the decrease of the total charge on the Pt-H moiety from  $-0.38 |e|$  to  $-0.10 |e|$  after the  $\text{CO}_2$  activation step. The charge on the  $-\text{OH}$  group, on the other hand, barely changes in the  $\text{CO}_2$  hydrogenation route, suggesting that the  $\text{CO}_2$  reduction and functionalization into formate occurs on the Pt-H moiety. The O atom in  $\text{H-Pt-OH}^-$  serves as another site for the initial interaction with  $\text{CO}_2$ . The negative charge on O is large ( $-1.04 |e|$ ), but NBO charge analysis reveals that it barely transfers to  $\text{CO}_2$  during the O/C interaction. The carbonation, which is not a redox reaction, occurs primarily on the  $-\text{OH}$  group, and the charge on the Pt-H moiety changes little in this route. This mechanism resembles the function of the ZnOH unit in a carbonic anhydrase.<sup>12i</sup> The charge analysis thus suggests that the hydrogenation and the carbonation routes proceed locally on the Pt-H and the O-H moieties, respectively, and each of the two moieties needs to possess appropriate negative charge for converting  $\text{CO}_2$  into other species. A charge analysis shows that in neutral  $\text{H-Pt-OH}$ , the charge on the Pt-H moiety is  $+0.38 |e|$ , making it unable to activate or hydrogenate  $\text{CO}_2$  (Fig. S4, ESI<sup>†</sup>). Therefore, electrons play a critical role in this molecular-level electrochemical  $\text{CO}_2$  reduction reaction, not only for enabling Pt atoms to activate  $\text{H}_2\text{O}$  activation, but also for keeping adequate negative charge on the Pt-H moiety in  $\text{H-Pt-OH}^-$  so  $\text{CO}_2$  reduction and hydrogenation can occur on it.

Fig. S5 (ESI<sup>†</sup>) presents a more complete reaction profile that also involves the route where  $\text{Pt}^-$  reacts with  $\text{CO}_2$  first then with  $\text{H}_2\text{O}$ . In this route,  $\text{CO}_2$  is activated and chemisorbed to  $\text{Pt}^-$  to form a  $\text{Pt-CO}_2^-$  complex. The  $\text{H}_2\text{O}$  molecule is physisorbed to this complex and gets activated *via* the breakage of the O-H

bond. The –OH group bonds to the Pt atom while the H atom bonds to the O atom of the CO<sub>2</sub> moiety, forming a HOPtCOOH<sup>−</sup> complex that contains a carboxyl group. While carboxyl has been commonly characterized in metal-surface electrochemical CO<sub>2</sub> reduction, in the context of gas-phase reactions where the catalyst is strictly single Pt anion and the participation from substrate is absent, this HOPtCOOH<sup>−</sup> complex will lead to the formation of formate products but not the carbonate products.

## Conclusions

To summarize, we demonstrate the activation and transformation of H<sub>2</sub>O and CO<sub>2</sub> mediated by electrons and single Pt atoms. The reaction mechanism is revealed by the synergy of mass spectrometry, photoelectron spectroscopy, and quantum chemical calculations. Specifically, a Pt atom captures an electron and activates H<sub>2</sub>O to form a H–Pt–OH<sup>−</sup> complex. This complex reacts with CO<sub>2</sub> *via* two different pathways to form formate, where CO<sub>2</sub> is hydrogenated, or to form bicarbonate, where CO<sub>2</sub> is carbonated. The overall formula of this reaction is identical to a typical electrochemical CO<sub>2</sub> reduction reaction on a Pt electrode. Since the reactants are electrons and isolated, single atoms and molecules, we term this reaction as a molecular-level electrochemical CO<sub>2</sub> reduction reaction. Mechanistic analysis reveals that the negative charge distribution on the Pt–H and the –OH moieties in H–Pt–OH<sup>−</sup> is critical for the hydrogenation and carbonation of CO<sub>2</sub>. The realization of the molecular-level CO<sub>2</sub> reduction reaction provides new insights into the design of novel catalysts for the electrochemical conversion of CO<sub>2</sub>.

## Methods

### Experimental methods

Anion photoelectron spectroscopy is conducted by crossing a beam of mass-selected negative ions with a fixed-frequency photon beam and energy-analyzing the resultant photodetached electrons. The photodetachment process is governed by the energy-conserving relationship:  $h\nu = \text{EBE} + \text{EKE}$ , where  $h\nu$  is the photon energy, EBE is the electron binding energy, and EKE is the electron kinetic energy. Our apparatus consists of a laser vaporization cluster anion source with an attached ligation cell, a time-of-flight mass spectrometer, a Nd:YAG photodetachment laser (operating at 266 nm), and a magnetic bottle electron energy analyzer with a resolution is  $\sim 35$  meV at 1 eV EKE.<sup>15</sup> Photoelectron spectra were calibrated against the well-known atomic transitions of atomic Cu<sup>−</sup>. The reaction among Pt<sup>−</sup>, H<sub>2</sub>O, and CO<sub>2</sub> was studied using a laser vaporization/reaction cell arrangement.<sup>16</sup> Atomic platinum anions were generated by laser vaporization of a pure platinum foil wrapped around an aluminum rod. The resultant plasma was cooled with a water vapor seeded helium gas mixture delivered by a pulsed valve, having a backing pressure of 80 psig. The resulting H–Pt–OH<sup>−</sup> then traveled through a reaction cell (4 mm diameter, 5 cm length), where it encountered CO<sub>2</sub>. CO<sub>2</sub> was

introduced into the reaction cell by a second pulsed valve, backed by 15 psig of pure CO<sub>2</sub> gas. The resulting [H–Pt–OH(CO)<sub>2</sub>]<sup>−</sup> anionic cluster was then mass-analyzed and mass-selected by the time-of-flight mass spectrometer and their photoelectron spectra measured.

### Computational methods

Geometries of intermediates and transition states were optimized at the density functional theory (DFT)/B3LYP level of theory using Gaussian16 package.<sup>17</sup> Harmonic vibrational frequency calculations carried out at the same level of theory to confirm the existence of only real frequencies for all energy minima, and one imaginary frequency for the transition states. Frequencies were used to estimate the zero-point energy corrections for all species. More accurate energies were obtained by performing single-point CCSD(T)<sup>18</sup> calculations using the B3LYP geometries. Obtained zero-point energies from DFT/B3LYP were added to calculate more accurate zero-point corrected CCSD(T) energies. All CCSD(T) calculations were performed using MOLPRO 2015 package.<sup>19</sup> For all calculations, the aug-cc-pVTZ (H, C, O)<sup>20,21</sup> and aug-cc-pVTZ-PP (Pt)<sup>22</sup> basis sets were employed. The inner 60 electrons (1s<sup>2</sup>2s<sup>2</sup>2p<sup>6</sup>3s<sup>2</sup>3p<sup>6</sup>3d<sup>10</sup>4s<sup>2</sup>4p<sup>6</sup>4d<sup>10</sup>4f<sup>14</sup>) of Pt were replaced with the Stuttgart relativistic pseudopotential.<sup>22</sup> To reproduce the photoelectron spectrum, we considered one Gaussian function for each stick of Fig. 2. The maximum was set equal to the calculated VDE and the full-width-of-half-maximum was approximated as (VDE–EA). The latter allows the onset of the Gaussian at around the EA value. The height of the Gaussian was fit to the experimental data. VDE is calculated as the energy difference between the anionic and neutral system using the anionic optimized geometry, and EBE is the same energy difference but using the optimal structure of each species. The VDE, EBE values, and intensities are given in the ESI.†

## Author contributions

Gaoxiang Liu and Isuru R. Ariyaratna contributed equally to this work.

## Conflicts of interest

There are no conflicts to declare.

## Acknowledgements

The experimental part of this material was supported by the Air Force Office of Scientific Research (AFOSR) under grant number, FA9550-19-1-0077 (KHB).

## References

- 1 B. Lu, Q. Liu and S. Chen, *ACS Catal.*, 2020, **10**, 7584.
- 2 Y. Chen, S. Ji, C. Chen, Q. Peng, D. Wang and Y. Li, *Joule*, 2018, **2**, 1242–1264.
- 3 C. Zhu, S. Fu, Q. Shi, D. Du and Y. Lin, *Angew. Chem., Int. Ed.*, 2017, **56**, 13944–13960.

- 4 G. Gao, Y. Jiao, E. R. Waclawik and A. Du, *J. Am. Chem. Soc.*, 2016, **138**, 6292–6297.
- 5 X. Su, X. F. Yang, Y. Huang, B. Liu and T. Zhang, *Acc. Chem. Res.*, 2018, **52**, 656–664.
- 6 X. Zhang, E. Lim, S. K. Kim and K. H. Bowen, *J. Chem. Phys.*, 2015, **143**, 174305.
- 7 G. Liu, S. Ciborowski, Z. Zhu, Y. Chen, X. Zhang and K. H. Bowen, *Phys. Chem. Chem. Phys.*, 2019, **21**, 10955–10960.
- 8 X. Zhang, G. Liu, K. Meiwes-Broer, G. Ganteför and K. Bowen, *Angew. Chem., Int. Ed.*, 2016, **55**, 9644–9647.
- 9 G. Liu, I. R. Ariyaratna, S. M. Ciborowski, Z. Zhu, E. Miliordos and K. H. Bowen, *J. Am. Chem. Soc.*, 2020, **142**, 21556–21561.
- 10 G. Liu, E. Miliordos, S. M. Ciborowski, M. Tschurl, U. Boesl, U. Heiz, X. Zhang, S. S. Xantheas and K. Bowen, *J. Chem. Phys.*, 2018, **149**, 221101.
- 11 O. P. Balaj, C. K. Siu, I. Balteanu, M. K. Beyer and V. E. Bondybey, *Chem. – Eur. J.*, 2004, **10**, 4822–4830.
- 12 (a) S. Zhou, J. Li, M. Schlangen and H. Schwarz, *Acc. Chem. Res.*, 2016, **49**, 494–502; (b) H. Schwarz, S. Shaik and J. Li, *J. Am. Chem. Soc.*, 2017, **139**, 17201–17212; (c) Y. X. Zhao, Z. Y. Li, Y. Yang and S. G. He, *Acc. Chem. Res.*, 2018, **51**, 2603–2610; (d) P. Armentrout, *J. Phys. Chem. A*, 2006, **110**, 8327–8338; (e) A. E. Green, J. Justen, W. Schöllkopf, A. S. Gentleman, A. Fielicke and S. R. Mackenzie, *Angew. Chem.*, 2018, **130**, 15038–15042; (f) G. E. Johnson, R. Mitric, M. Nössler, E. C. Tyo, V. Bonacic-Koutecky and A. Castleman Jr., *J. Am. Chem. Soc.*, 2009, **131**, 5460–5470; (g) G. Deng, S. Pan, G. Wang, L. Zhao, M. Zhou and G. Frenking, *Angew. Chem., Int. Ed.*, 2020, **59**, 18201–18207; (h) J. Jian, X. Wu, M. Chen and M. Zhou, *J. Am. Chem. Soc.*, 2020, **142**, 10079–10086; (i) H. Schwarz, *Coord. Chem. Rev.*, 2017, **334**, 112–123.
- 13 (a) G. Liu, Z. Zhu, M. Marshall, M. Blankenhorn and K. H. Bowen, *J. Phys. Chem. A*, 2021, **125**, 1747–1753; (b) G. Liu, P. Poths, X. Zhang, Z. Zhu, M. Marshall, M. Blankenhorn, A. N. Alexandrova and K. H. Bowen, *J. Am. Chem. Soc.*, 2020, **142**, 7930–7936; (c) G. Liu, Z. Zhu, S. M. Ciborowski, I. R. Ariyaratna, E. Miliordos and K. H. Bowen, *Angew. Chem., Int. Ed.*, 2019, **131**, 7855–7859; (d) S. M. Lang, T. M. Bernhardt, V. Chernyy, J. M. Bakker, R. N. Barnett and U. Landman, Selective C–H bond cleavage in methane by small gold clusters, *Angew. Chem.*, 2017, **129**, 13591–13595.
- 14 L. X. Jiang, C. Zhao, X. N. Li, H. Chen and S. G. He, *Angew. Chem., Int. Ed.*, 2017, **56**, 4187–4191.
- 15 X. Zhang, G. Liu, G. Ganteför, K. H. Bowen and A. N. Alexandrova, *J. Phys. Chem. Lett.*, 2014, **5**, 1596–1601.
- 16 G. Liu, S. M. Ciborowski and K. H. Bowen, *J. Phys. Chem. A*, 2017, **121**, 5817–5822.
- 17 M. J. Frisch, G. W. Trucks, H. B. Schlegel, G. E. Scuseria, M. A. Robb, J. R. Cheeseman, G. Scalmani, V. Barone, G. A. Petersson, H. Nakatsuji *et al.* *Gaussian 16 Rev. C.01*, Wallingford CT, 2016.
- 18 K. Raghavachari, G. W. Trucks, J. A. Pople and M. A. Head-Gordon, *Chem. Phys. Lett.*, 1989, **157**, 479–483.
- 19 H. J. Werner, P. J. Knowles, G. Knizia, F. R. Manby, M. Schütz, P. Celani, W. Györffy, D. Kats, T. Korona, R. Lindh, *et al.*, *MOLPRO, version 2015.1*, a package of ab initio programs, 2015.
- 20 R. A. Kendall, T. H. Dunning and R. J. Harrison, *J. Chem. Phys.*, 1992, **96**, 6796–6806.
- 21 T. H. Dunning, *J. Chem. Phys.*, 1989, **90**, 1007–1023.
- 22 D. Figgen, K. A. Peterson, M. Dolg and H. Stoll, *J. Chem. Phys.*, 2009, **130**, 164108.